The Astrophysical Journal, 763:89 (6pp), 2013 February 1 doi:10.1088/0004-637X/763/2/89

SIMULTANEOUS CONSTRAINTS ON THE NUMBER AND MASS OF RELATIVISTIC SPECIES

Signe Riemer-Sørensen[1], David Parkinson[1], Tamara M. Davis[1], and Chris Blake[2]
[1] School of Mathematics and Physics, University of Queensland, Brisbane, QLD 4072, Australia; signe@physics.uq.edu.au
[2] Centre for Astrophysics & Supercomputing, Swinburne University of Technology, P.O. Box 218, Hawthorn, VIC 3122, Australia

Received 2012 October 8; accepted 2012 December 3; published 2013 January 14

ABSTRACT

Recent indications from both particle physics and cosmology suggest the possible existence of more than three neutrino species. In cosmological analyses the effects of neutrino mass and number of species can in principle be disentangled for fixed cosmological parameters. However, since we do not have perfect measurements of the standard Λ cold dark matter model parameters, some correlation remains between the neutrino mass and number of species, and both parameters should be included in the analysis. Combining the newest observations of several cosmological probes (cosmic microwave background, large-scale structure, expansion rate), we obtain $N_{\rm eff} = 3.58^{+0.15}_{-0.16}(68\%\,{\rm CL})^{+0.55}_{-0.53}(95\%\,{\rm CL})$ and $\sum m_\nu < 0.60\,{\rm eV}(95\%\,{\rm CL})$, which are currently the strongest constraints on $N_{\rm eff}$ and $\sum m_\nu$ from an analysis including both parameters. The preference for $N_{\rm eff} > 3$ is at the 2σ level.

Key words: cosmology: observations – neutrinos

Online-only material: color figures

1. INTRODUCTION

Neutrinos are the lightest massive known particles, and despite the fact that we know they have mass, they are treated as exactly massless by the Standard Model of particle physics. Neutrino oscillation experiments using solar, atmospheric, and reactor neutrinos have measured mass differences between the three Standard Model species[3] to be $\Delta m^2_{32} = |(2.43^{+0.12}_{-0.08}) \times 10^{-3}|\ {\rm eV}^2$ and $\Delta m^2_{21} = (7.50 \pm 0.20) \times 10^{-5}\ {\rm eV}^2$ (Fukuda et al. 1998; Beringer et al. 2012). The Mainz and Troitsk experiments have limited the electron neutrino mass to less than 2 eV (95% CL; Kraus et al. 2005; Aseev et al. 2011), and for the special case of Majorana neutrinos, the limit from the Heidelberg–Moscow experiment is 0.35 eV (Klapdor-Kleingrothaus & Krivosheina 2006), but no current laboratory experiment has the sensitivity to measure the absolute neutrino mass.

The oscillation data from short baseline experiments exhibit some tension allowing for, or even preferring, the existence of additional neutrino species. Depending on the exact analysis, the preferred scenarios include either one or two sterile neutrinos in addition to the three normal ones (3+1 or 3+2; Kopp et al. 2011; Mention et al. 2011; Giunti & Laveder 2011), e.g., Mention et al. (2011) favor 3+1 over 3 at 99.8% confidence.

Observations of the cosmic microwave background (CMB) also seem to favor possible additional species of radiation to be present at the time of decoupling over and above that provided by the photon density and three Standard Model neutrinos; most notably the results from the Atacama Cosmology Telescope (Dunkley et al. 2011) of $N_{\rm eff} = 5.3 \pm 1.3$ but other authors, e.g., Komatsu et al. (2011), Hou et al. (2011), and Keisler et al. (2011), find a similar preference at the 1σ–2σ level. $N_{\rm eff}$ is the parameterization of this radiation in terms of the effective number of neutrino species. By analogy to dark energy and dark matter, this extra radiation is often dubbed dark radiation.

The neutrino oscillation results favor a large mass difference (e.g., Kopp et al. 2011) providing a lower limit on the sterile neutrino mass of the order of 1 eV, which is incompatible with cosmological mass constraints from combinations of CMB and large-scale structure (LSS) measurements ($\sum m_\nu <$ 0.3–0.6 eV, e.g., Riemer-Sørensen et al. 2012; Archidiacono et al. 2012; Joudaki et al. 2012), but it has been shown that factors such as initial lepton asymmetry can possibly alleviate these constraints by introducing a non-thermal neutrino velocity spectrum and thereby avoiding the LSS mass constraints (Hannestad et al. 2012).

Within the last couple of years, many publications have addressed the issues of neutrino mass and effective number of neutrinos separately (Moresco et al. 2012b; Xia et al. 2012; de Putter et al. 2012; Riemer-Sørensen et al. 2012) but very few consider the correlation between the two (exceptions are Hamann et al. 2010a, 2010b). In this paper we address these correlations and demonstrate that due to imperfect measurements of the standard Λ cold dark matter (ΛCDM) parameters, the two parameters are not entirely independent but should be addressed simultaneously. Section 2 explains the physical and observable effects of $N_{\rm eff}$ and $\sum m_\nu$; Sections 3 and 4 describe the data and methods used to obtain the results of cosmological fits which are presented in Section 5.

2. PHYSICAL AND OBSERVABLE EFFECTS

This section briefly explains the physical effects of $\sum m_\nu$ and $N_{\rm eff}$ and how they can be measured. The parameter that is probed directly by cosmological analyses is not the neutrino mass, but the neutrino density, ρ_ν, which can be expressed in terms of the mass (Lesgourgues & Pastor 2006):

$$\Omega_\nu = \frac{\rho_\nu}{\rho_c} = \frac{\sum_{i=1}^{N_\nu} m_{\nu,i}}{93.14\,{\rm eV}h^2}, \quad (1)$$

where ρ_c is the critical energy density for a flat Universe, and N_ν is the number of massive neutrino states. Because of the smallness of the measured mass differences relative to the upper limits, it is reasonable to assume that if the individual neutrino masses are near the upper limit, they are effectively equal.

[3] Technically they are not Standard Model neutrinos because they have mass, but here we refer to the ν_e, ν_μ, and ν_τ as Standard Model, and any additional species as sterile.

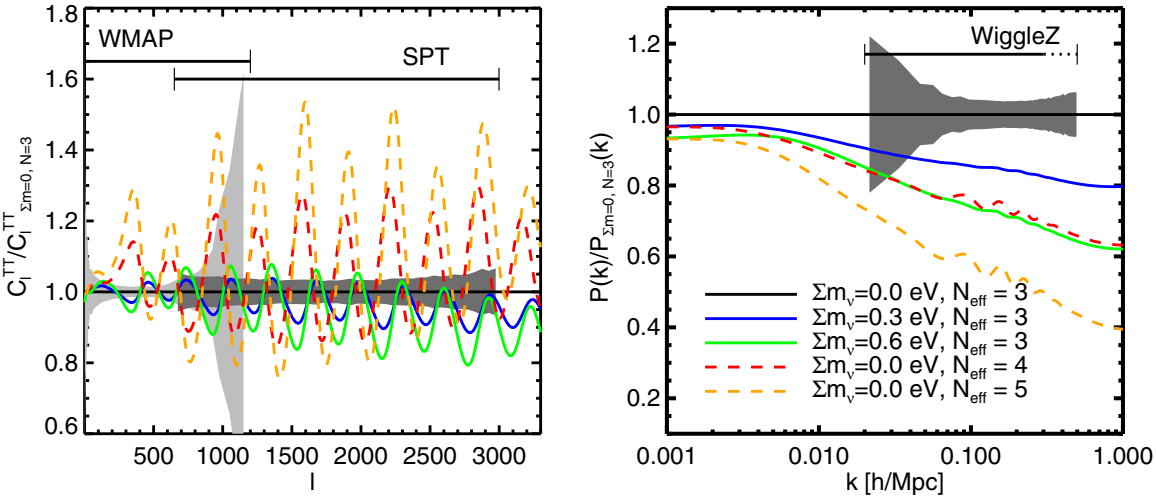

Figure 1. Illustration of how the CMB and matter power spectra change for varying neutrino mass (solid lines) and effective number of neutrinos (dashed lines) fixing all other parameters (to *WMAP* 7 yr values for ΛCDM). $\sum m_\nu$ does not affect the CMB power spectrum much, but changes the matter power spectrum significantly. The effect of $N_{\rm eff}$ is clearly visible for small scales (high values of l) in the CMB power spectrum, and the two parameters are clearly degenerate in particular for the matter power spectrum. The shaded regions indicate the normalized uncertainties of current experiments.

(A color version of this figure is available in the online journal.)

2.1. Massive Neutrino Effects on the Expansion

Due to the weakness of the weak interaction, the neutrinos decouple early from the tightly coupled baryon–photon fluid ($T = 2$–4 MeV), while the expansion is still dominated by radiation. If $\sum m_\nu > 1$ eV, the neutrinos become non-relativistic before recombination. However, cosmological constraints already indicate $\sum m_\nu < 1$ eV, so the neutrinos become non-relativistic after recombination, and while they are relativistic their energy density contributes as radiation rather than matter. The presence of "neutrino radiation" affects the expansion rate and changes the time of the matter-radiation equality. The latter determines when the density perturbations can begin to collapse gravitationally and structures can evolve. The higher $\sum m_\nu$ or $N_{\rm eff}$, the higher the radiation density and the later the equality takes place. Changing the expansion rate and time of the matter-radiation equality has some measurable consequences described below and illustrated in Figure 1.

1. The position of the peak of the matter power spectrum is determined by the particle horizon length scale at the time of matter-radiation equality. Moving the equality to later times shifts the peak to larger scales.
2. The expansion rate determines the time available for sound waves to propagate in the baryon–photon fluid before recombination, which will imprint on the baryon acoustic oscillation (BAO) scale measurable from both the CMB and the LSS. Increasing the expansion rate will move the BAO peak to smaller scales.
3. Delaying matter-radiation equality enhances the ratio of even to odd peaks in the CMB power spectrum because the dark matter potentials have a longer time to grow, and thereby increasing the BAO amplitude (the gravitational potentials are deeper, but the photon restoring force is the same). It also increases the early Sachs–Wolfe effect, which enhances the overall normalization of the CMB power spectrum.
4. Similar to the photons, the neutrinos have a viscosity that generates damping on small scales through anisotropic stress and free-streaming effects (Hu et al. 1998). Fluctuations in the neutrino density lead to a shift in the positions of the acoustic peaks in the CMB.
5. Changing the expansion rate can significantly affect the big bang nucleosynthesis (BBN) leading to different deuterium and helium abundances than the observationally confirmed predictions of standard BBN (Lesgourgues & Pastor 2006; Steigman 2012).

2.2. Massive Neutrino Effects on Structure Formation

When the neutrinos have decoupled, their thermal velocities decay adiabatically as (Komatsu et al. 2011)

$$v_{\rm thermal} = 151(1+z)(1\,{\rm eV}/m_\nu)\,{\rm km\,s^{-1}}. \quad (2)$$

When they become non-relativistic they behave as a species of warm/hot dark matter, suppressing density fluctuations on scales smaller than their free-streaming length (at the time when they become non-relativistic; Lesgourgues & Pastor 2006):

$$k_{\rm FS} = \sqrt{\frac{3}{2}}\frac{H(t)}{v_{\rm thermal}(t)(1+z)} \quad (3)$$

$$\approx 0.82\frac{\sqrt{\Omega_\Lambda + \Omega_m(1+z)^3}}{(1+z)^2}\left(\frac{m_\nu}{1\,{\rm eV}}\right)h{\rm Mpc}^{-1}. \quad (4)$$

Neutrinos cannot cluster on scales smaller than their free-streaming length and consequently the density fluctuations are suppressed by a factor proportional to the neutrino density. This is observable in the density power spectrum as a suppression of structure on small scales (see the right part of Figure 1). However, the presence of neutrinos also enhances the density perturbations (by adding to the radiation density for fixed $\Omega_{\rm m}$), which boosts structure formation in general, so for higher $N_{\rm eff}$, σ_8 will increase (Hou et al. 2011).

The evolution of the density perturbations can be predicted by solving the coupled set of Einstein and Boltzman equations. For small density perturbations, the linearized equations are

sufficient (e.g., using CAMB[4]), but when the density perturbations grow sufficiently large, the higher-order, nonlinear terms become important and have to be included, which is computationally very intensive (and not yet solved analytically). Instead one has to rely on second-order perturbation theory (e.g., Saito et al. 2009; Taruya et al. 2012) or simulations (e.g., Smith et al. 2003; Jennings et al. 2010).

Numerical solutions show that for $f_\nu = \Omega_\nu/\Omega_m < 0.07$ the suppression is $\delta P/P = -8 f_\nu$ for linear structure formation (Hu et al. 1998) and the effect increases for nonlinear structure formation ($8 \rightarrow 9.6$; Brandbyge et al. 2008, 2010; Brandbyge & Hannestad 2009; Viel et al. 2010; Agarwal & Feldman 2011).

The signature of free-streaming massive neutrinos can be detected in both the power spectrum of CMB temperature anisotropies and in the (matter) density power spectrum of LSS. As illustrated in Figure 1, the larger the neutrino mass, the more prominent these effects on the power spectra of the CMB and LSS.

The density power spectrum can be traced either through galaxies (galaxy power spectrum) or through the absorption lines from neutral hydrogen clouds along the line of sight to distant quasars (Lyα forest power spectrum). The neutrinos affect the total matter power spectrum, which may differ slightly from the tracer power spectrum that we actually measure. Depending on the tracer, the bias, $P_{\rm obs} = b^2 P_{\rm m}$, might be scale-dependent or scale-independent (Schulz & White 2006).

Another effect that is important for spectroscopic galaxy surveys is the redshift space distortions caused by galaxies falling into the gravitational potential of galaxy clusters (Kaiser 1987; Percival & White 2009). As structure formation becomes nonlinear, so do the redshift space distortions (Jennings et al. 2010; Marulli et al. 2011).

3. DATA

For the analysis presented here we have used the following publicly available data sets.

CMB$_{WMAP}$. The CMB as observed by *Wilkinson Microwave Anisotropy Probe* (*WMAP*) from the 7 year data release[5] (Komatsu et al. 2011).

CMB$_{\rm SPT}$. The CMB as observed by the South Pole Telescope[6] (SPT; Keisler et al. 2011).

H_0. A Gaussian prior of $H_0 = 73.8 \pm 2.4\ {\rm km\,s^{-1}\,Mpc^{-1}}$ on the Hubble parameter value today from Riess et al. (2011). A recent analysis based on re-calibration of the cepheids found $H_0 = 74.3 \pm 2.1\ {\rm km\,s^{-1}\,Mpc^{-1}}$ (Freedman et al. 2012), which is slightly larger than the value adopted here driving the value of $N_{\rm eff}$ upward. However, the tightest constraints presented here do not rely on the H_0 measurement but the BAO and supernova (SN) to constrain the expansion history.

$H(z)$. The expansion history of the Universe as measured with passively evolving galaxies at $z < 1.75$. The combined sample of Simon et al. (2005), Stern et al. (2010), and Moresco et al. (2012a) as given in Moresco et al. (2012b). The main potential systematic error lies in the modeling of the stellar populations. However, we are reassured by the fact that the resulting expansion history is consistent with $H(z)$ as measured from the Alcock–Paczynski test with the WiggleZ galaxies (Blake et al. 2012), which is prone to entirely different systematics. This agreement puts an upper limit on the possible systematics on the $H(z)$ measurements.

BAO. The BAO scale measured at $z = 0.106$ ($r_s/D_V = 0.336 \pm 0.015$) from the Six Degree Field Galaxy Survey (6dFGS; Beutler et al. 2011), the reconstructed value at $z = 0.35$ ($r_s/D_V = 0.1126 \pm 0.0022$) from Sloan Digital Sky Survey (SDSS) luminous red galaxies (LRGs; Padmanabhan et al. 2012), and $z = 0.57$ ($r_s/D_V = 0.0732 \pm 0.0012$) from the Baryon Oscillation Spectroscopic Survey (BOSS; Anderson et al. 2012). The measurements of r_s/D_V are independent of the assumed fiducial values of $N_{\rm eff}$ (as they cancel out).

SN. Type Ia SNe as observed by the three-year SuperNova Legacy Survey (SNLS; Guy et al. 2010; Sullivan et al. 2011; Conley et al. 2011). We use the SNLS data which are a uniform sample of SN observed with a single telescope, avoiding many of the potential systematics errors between individual SNe, and consequently free from some of the light-curve fitting issues that Joudaki et al. (2012) pointed out between the Union2 and SDSS SN data sets.

$P(k)$. The WiggleZ Dark Energy Survey power spectrum[7] as described in Parkinson et al. (2012). The main systematic uncertainty is the modeling of the nonlinear matter power spectrum. The robustness of the WiggleZ analysis was thoroughly tested as discussed in Parkinson et al. (2012).

3.1. Comments on Data Combinations

WMAP and SPT are highly complementary observations of the CMB. *WMAP* is a full sky survey including the largest scales (multipole moments $l = 2$–1200) while SPT is a high-resolution small-scale survey ($l = 650$–2999) very sensitive to effects of changing $N_{\rm eff}$ (see the left panel of Figure 1).

The LSS can be included either in the form of the BAO scale or the full power spectrum shape. To be conservative, we do not include both the BAO distance measurement and the power spectrum shape data from the same survey since we do not know the correlation between the two. For our main result we use the BAO scale from 6dFGS, SDSS, and BOSS, and the full WiggleZ power spectrum. We have tested that the results from this setup are very similar to using the full power spectrum shape from both SDSS and WiggleZ. This is because the constraints are limited by the determination of the ΛCDM parameters rather than by the observational determination of the slope of the galaxy power spectrum. The precise determination of the BAO scale strengthens the constraints on the ΛCDM parameters, which improves the $\sum m_\nu$ and $N_{\rm eff}$ constraints by breaking degeneracies. Therefore, including some BAO data is more important than including the full power spectrum shape for all LSS data.

Whenever a data set introduces extra parameters, e.g., galaxy bias for the matter power spectra, we marginalize over these extra parameters.

4. METHOD

We fit the data to a standard flat ΛCDM cosmology with the following parameters: the physical baryon density ($\Omega_{\rm b}h^2$),

[4] http://camb.info.

[5] Available from http://lambda.gsfc.nasa.gov.

[6] Available from http://pole.uchicago.edu/public/data/keisler11/.

[7] Available from http://smp.uq.edu.au/wigglez-data.

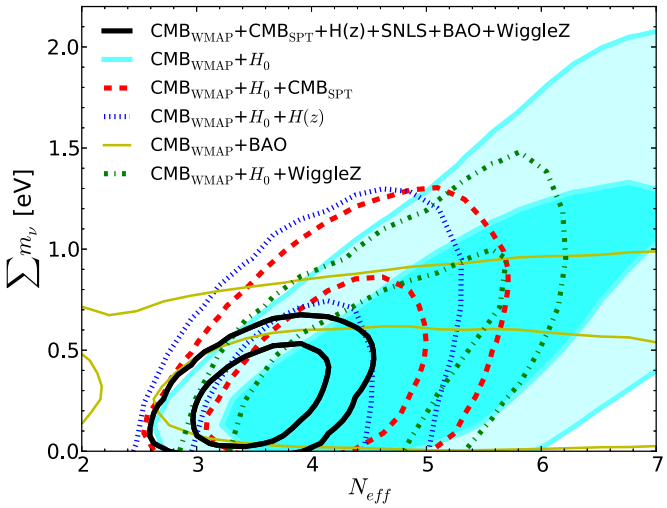

Figure 2. The 68% and 95% CL contours in the $N_{\rm eff}$–$\sum m_\nu$ parameter space of fitting a ΛCDM+$\sum m_\nu$+$N_{\rm eff}$ model to a selection of data combinations.
(A color version of this figure is available in the online journal.)

the physical cold dark matter density ($\Omega_{\rm dm}h^2$), the Hubble parameter at $z = 0$ (H_0), the optical depth to reionization (τ), the amplitude of the primordial density fluctuations (A_s), and the primordial power spectrum index (n_s). In addition, we vary the effective number of relativistic degrees of freedom ($N_{\rm eff} = N_\nu + \Delta N_{\rm eff}$) and the sum of neutrino masses ($\sum m_\nu = N_\nu m_\nu$), where N_ν is the number of massive neutrinos usually taken to be $N_\nu = 3.046$ and the 0.046 accounts for the neutrino energies that arise due to the residual heating provided by the e^+e^- annihilations after the neutrino decoupling (Mangano et al. 2005).

We sample the parameter space using the Markov Chain Monte Carlo sampler[8] CosmoMC (Lewis & Bridle 2002). Details on the specific modules can be found in Parkinson et al. (2012) and on the WiggleZ Web site.[5]

The probability distributions are calculated by marginalizing over the density of points in the chains. Because the distributions can be non-Gaussian, the 2σ uncertainties can be larger than two times the 1σ uncertainties.

5. RESULTS AND DISCUSSION

From fitting ΛCDM+$\sum m_\nu$+$N_{\rm eff}$ to CMB$_{WMAP}$ + CMB$_{\rm SPT}$ + WiggleZ + $H(z)$ + BAO + SN, we obtain $N_{\rm eff} = 3.58^{+0.15}_{-0.16}$ (68% CL)$^{+0.55}_{-0.53}$(95% CL) and $\sum m_\nu < 0.60$ eV(95% CL) shown in Figures 2 and 3. This represents a preference for more than three neutrino species at 95% confidence.

5.1. Comparison to ΛCDM

Figure 4 shows the resulting contours from fitting ΛCDM+$\sum m_\nu$+$N_{\rm eff}$ to CMB$_{WMAP}$ + CMB$_{\rm SPT}$ + WiggleZ + $H(z)$ + BAO + SN (solid black), compared to fitting a pure ΛCDM model (dashed red), ΛCDM+$\sum m_\nu$ (dotted blue), and ΛCDM+$N_{\rm eff}$ (dot-dashed green) to the same data. Naturally the constraints are tighter for pure ΛCDM, since there are fewer parameters to constrain, but overall the constraints are consistent for all parameters. Adding $\sum m_\nu$ to the fit does not change the ΛCDM parameters or uncertainties significantly, whereas

[8] http://cosmologist.info/

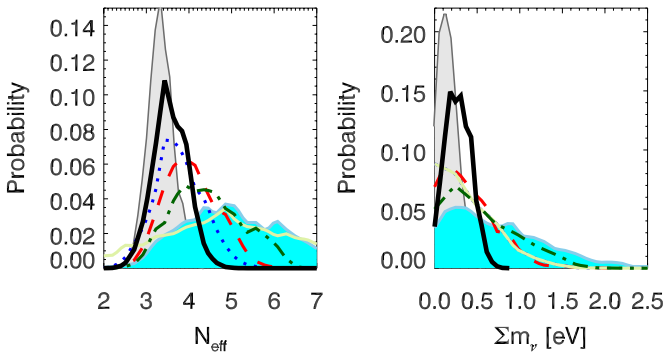

Figure 3. One-dimensional probability distributions for $N_{\rm eff}$ and $\sum m_\nu$ of fitting a ΛCDM+$\sum m_\nu$+$N_{\rm eff}$ model to a selection of data combinations (same colors as in Figure 2). The gray shaded area indicates the probability distribution when correlations are neglected by fixing $\sum m_\nu = 0$ (left) and $N_{\rm eff} = 3.046$ (right).
(A color version of this figure is available in the online journal.)

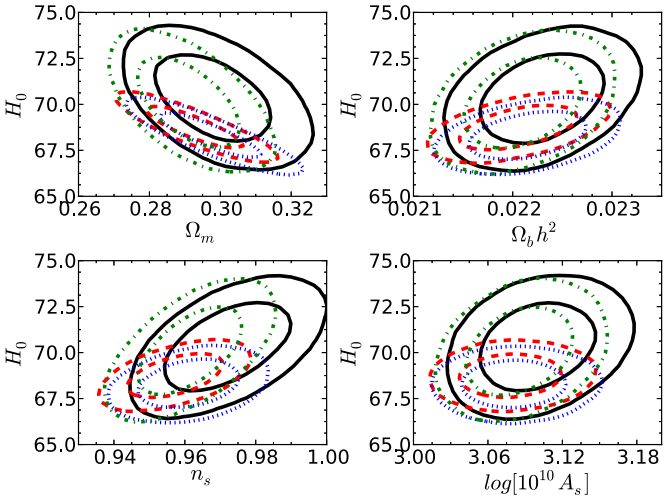

Figure 4. The 68% and 95% CL contours for fitting ΛCDM+$\sum m_\nu$+$N_{\rm eff}$ (solid black), ΛCDM+$\sum m_\nu$ (dotted blue), ΛCDM+$N_{\rm eff}$ (dot-dashed green), and ΛCDM (dashed red) models to CMB$_{WMAP}$ + CMB$_{\rm SPT}$ + WiggleZ + $H(z)$ + BAO + SN data. The resulting contours are consistent with each other for all parameters.
(A color version of this figure is available in the online journal.)

Table 1
Likelihoods for Models Fit to CMB$_{WMAP}$ + CMB$_{\rm SPT}$ + WiggleZ + $H(z)$ + BAO + SN

Model	$-\log(\mathcal{L})$	Free Parameters
ΛCDM	4379.50	6
ΛCDM+$\sum m_\nu$	4379.48	6+1
ΛCDM+$N_{\rm eff}$	4379.40	6+1
ΛCDM+$\sum m_\nu$+$N_{\rm eff}$	4378.48	6+2

adding $N_{\rm eff}$ increases the values and uncertainties of H_0. Adding both parameters increases the preferred values of H_0 and n_s but also the uncertainties, so the values remain consistent with the pure ΛCDM case. The shift can be understood as follows: increasing H_0 changes the height of the peaks in the CMB, as it corresponds to increasing the physical matter density. Changing $N_{\rm eff}$ recovers the details of the CMB peaks (because the original ratio of matter to radiation is recovered, restoring the details of Silk damping), but with too much power on large scales due to the integrated Sachs-Wolfe effect. This shifts the primordial power spectrum from very red ($n_s = 0.96$) to slightly less red (0.98–1.0). The likelihoods for each of the best fits given in Table 1 are very similar for the four model combinations

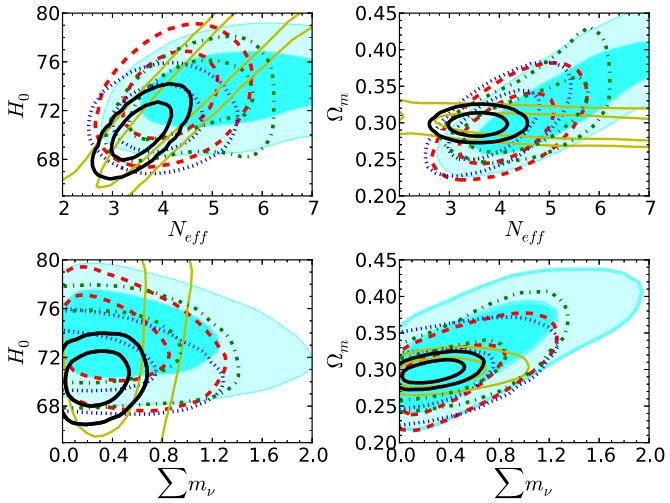

Figure 5. Results of fitting a ΛCDM+$\sum m_\nu$+$N_{\rm eff}$ model to a selection of data combinations (same colors as in Figure 2).

(A color version of this figure is available in the online journal.)

without a cosmological preference for any of the models, but we know from oscillation experiments that massive neutrinos exist and consequently should be included in the model from a physical argument.

5.2. Combinations and Degeneracies

It is clear from the $\sum m_\nu$–$N_{\rm eff}$ contours in Figure 2 that unless all data sets are included, the two parameters are correlated. The tightest constraints come from the combination of CMB$_{WMAP}$ + CMB$_{\rm SPT}$ + WiggleZ + $H(z)$ + BAO + SN. Figure 5 demonstrates the degeneracies in the planes of $\sum m_\nu$ − $N_{\rm eff}$, and H_0 − $\Omega_{\rm m}$. When all the data are combined, there is a significant correlation between H_0 and $N_{\rm eff}$, and a mild correlation between $\sum m_\nu$ and $\Omega_{\rm m}$. Lowering H_0 shifts $N_{\rm eff}$ back toward the expected value of three. For the full data combination, the best-fit value of $H_0 = 70.3 \pm 1.5\ {\rm km\,s^{-1}\,Mpc^{-1}}$ is driven mainly by the BAO measurements. It is slightly smaller than the $H_0 = 73.8 \pm 2.4\ {\rm km\,s^{-1}\,Mpc^{-1}}$ measured by Riess et al. (2011), but consistent within 2σ. Forcing H_0 up to match the SN measurements would lead to an even higher best-fit value of $N_{\rm eff}$.

As seen from the shaded region in Figure 5, the data combinations favoring the highest value of $N_{\rm eff}$ are CMB$_{WMAP}$+ H_0 and CMB$_{WMAP}$ + BAO. Adding additional data sets pushes the value of $N_{\rm eff}$ down. This indicates that the high value is driven by the *WMAP* data, and the other data sets mainly serve to reduce the uncertainty. Any underestimation of the systematic uncertainties in the additional data sets will not affect the final conclusion significantly if the result is mainly driven by the *WMAP* data. However, if there are systematic uncertainties in the *WMAP* data, those errors will propagate through the combined analyses presented here.

At the present, LSS (e.g., WiggleZ and SDSS) does not constrain $N_{\rm eff}$ uniquely because the turnover of the power spectrum is not well measured, which leaves some correlation between $\Omega_{\rm m}$, $\sum m_\nu$, and $N_{\rm eff}$ (see Figure 1), but inclusion of the power spectrum improves on $\sum m_\nu$ from the small-scale suppression.

The $H(z)$ data do not add much to the neutrino mass constraints, but because it constrains the expansion history, it improves on the limits on $N_{\rm eff}$ as discussed in Moresco et al. (2012b).

5.3. Nucleosynthesis

There have been a number of recent attempts to derive $N_{\rm eff}$ from BBN alone (e.g., Mangano & Serpico 2011; Pettini & Cooke 2012), which all seem to be consistent with $N_{\rm eff} = 3$. Analyses combining BBN and CMB seem to prefer $N > 3$ (e.g., Nollett & Holder 2011; Hamann et al. 2011). It is concerning that the preference for $N_{\rm eff} > 3$ is present in all analyses including CMB, but not preferred by BBN alone. This could indicate a systematic error in one of the data sets. However, BBN alone relies on very few and notoriously difficult measurements of the deuterium and helium fractions.

The difference between the results could also be interpreted as potential tension between $N_{\rm eff}$ measured at two different epochs (BBN and recombination), where we naively would expect $N_{\rm eff}$ to be the same. A temporal variation can be explained theoretically by a decaying particle (Boehm et al. 2012) but currently there is no experimental evidence for the existence of such a particle.

5.4. Beyond ΛCDM+$\sum m_\nu$+$N_{\rm eff}$

Other physical effects such as curvature, varying equation of state, running of the spectral index, etc., could mimic $N_{\rm eff} > 3$ if not properly accounted for in the modeling. Joudaki (2012) demonstrated that the deviation from $N_{\rm eff} = 3.046$ is diminished if allowing for curvature, varying equation of state, running of the spectral index, and/or the helium fraction by fitting to CMB$_{WMAP}$, CMB$_{\rm SPT}$, BAO scale from SDSS and 2dFGS, H_0 from *Hubble Space Telescope*, and SN from Union2. However, for all parameter combinations the preferred value of $N_{\rm eff}$ was still above three, and only when more than one extra extension of the ΛCDM cosmology (e.g., curvature *and* varying equation of state in addition to $N_{\rm eff}$ and $\sum m_\nu$) were considered, did the preferred value of $N_{\rm eff}$ become consistent with three within one standard deviation. We take this as an indication that one extension alone does not explain the preference for $N_{\rm eff} \neq 3$.

5.5. Future

Measuring the position of the peak of the matter power spectrum (the turnover) would give another handle on $N_{\rm eff}$. G. B. Poole et al. (2013, in preparation) predict that a Euclid-like galaxy survey will be able to constrain $N_{\rm eff}$ to approximately 20% independently of the CMB. However, the position of the turnover can be degenerate with neutrino hierarchy effects (Wagner et al. 2012). The degeneracies between $\sum m_\nu$, $N_{\rm eff}$, and the hierarchy allow for a measurement of either of them if the remaining parameters can be "fixed" by independent data.

If $N_{\rm eff}$ can be measured with sufficiently high precision, eventually it will be possible to measure the thermal distortion of the neutrino spectrum (the 0.046).

Any neutrino-like behaving particle, including sterile neutrinos and axions, etc., which decouple early when relativistic and become non-relativistic, can mimic the effect of the neutrinos. If the value of $N_{\rm eff} > 3$ is due to a particle, the result points toward physics beyond the Standard Model, and its existence it will have to be confirmed by a particle physics laboratory experiment. If no sterile neutrinos are found in laboratory experiments, the cosmological preference for additional species may indicate a lack of understanding of early Universe physics or possible observational systematics.

6. CONCLUSION

Due to imperfect measurements of the ΛCDM parameters, $\sum m_\nu$ and $N_{\rm eff}$ are not entirely independent parameters and should be fitted simultaneously in cosmological analyses. Performing such fit of ΛCDM+$\sum m_\nu$+$N_{\rm eff}$ to a combination of cosmological data sets leads to a 2σ preference for $N_{\rm eff} > 3$ with $N_{\rm eff} = 3.58^{+0.55}_{-0.53}$ (95% CL) and $\sum m_\nu < 0.60\,{\rm eV}$ (95% CL), which are currently the strongest constraints on $N_{\rm eff}$ from cosmological analysis simultaneously fitting for $N_{\rm eff}$ and $\sum m_\nu$.

REFERENCES

Agarwal, S., & Feldman, H. A. 2011, MNRAS, 410, 1647
Anderson, L., Aubourg, E., Bailey, S., et al. 2012, MNRAS, 427, 3435
Archidiacono, M., Fornengo, N., Giunti, C., & Melchiorri, A. 2012, PhRvD, 86, 065028
Aseev, V. N., Belesev, A. I., Berlev, A. I., et al. 2011, PhRvD, 84, 112003
Beringer, J., Arguin, J.-F., Barnett, R. M., et al. 2012, PhRvD, 86, 010001
Beutler, F., Blake, C., Colless, M., et al. 2011, MNRAS, 416, 3017
Blake, C., Brough, S., Colless, M., et al. 2012, MNRAS, 425, 405
Boehm, C., Dolan, M. J., & McCabe, C. 2012, JCAP, 12, 027
Brandbyge, J., & Hannestad, S. 2009, JCAP, 05, 002
Brandbyge, J., Hannestad, S., Haugbølle, T., & Thomsen, B. 2008, JCAP, 08, 020
Brandbyge, J., Hannestad, S., Haugbølle, T., & Wong, Y. Y. Y. 2010, JCAP, 09, 014
Conley, A., Guy, J., Sullivan, M., et al. 2011, ApJS, 192, 1
de Putter, R., Mena, O., Giusarma, E., et al. 2012, ApJ, 761, 12
Dunkley, J., Hlozek, R., Sievers, J., et al. 2011, ApJ, 739, 52
Freedman, W. L., Madore, B. F., Scowcroft, V., et al. 2012, ApJ, 758, 24
Fukuda, Y., Hayakawa, T., Ichihara, E., et al. 1998, PhRvL, 81, 1562
Giunti, C., & Laveder, M. 2011, PhRvD, 84, 093006
Guy, J., Sullivan, M., Conley, A., et al. 2010, A&A, 523, A7
Hamann, J., Hannestad, S., Lesgourgues, J., et al. 2010a, JCAP, 07, 022
Hamann, J., Hannestad, S., Raffelt, G. G., et al. 2010b, PhRvL, 105, 181301
Hamann, J., Hannestad, S., Raffelt, G. G., & Wong, Y. Y. Y. 2011, JCAP, 09, 034
Hannestad, S., Tamborra, I., & Tram, T. 2012, JCAP, 07, 025
Hou, Z., Keisler, R., Knox, L., Millea, M., & Reichardt, C. 2011, arXiv:1104.2333
Hu, W., Eisenstein, D. J., & Tegmark, M. 1998, PhRvL, 80, 5255
Jennings, E., Baugh, C. M., & Pascoli, S. 2010, MNRAS, 401, 2081
Joudaki, S. 2012, arXiv:1202.0005
Joudaki, S., Abazajian, K. N., & Kaplinghat, M. 2012, arXiv:1208.4354
Kaiser, N. 1987, MNRAS, 227, 1
Keisler, R., Reichardt, C. L., Aird, K. A., et al. 2011, ApJ, 743, 28
Klapdor-Kleingrothaus, H. V., & Krivosheina, I. V. 2006, MPLA, 21, 1547
Komatsu, E., Smith, K. M., Dunkley, J., et al. 2011, ApJS, 192, 18
Kopp, J., Maltoni, M., & Schwetz, T. 2011, PhRvL, 107, 091801
Kraus, Ch., Bornschein, B., Bornschein, L., et al. 2005, EPJC, 40, 447
Lesgourgues, J., & Pastor, S. 2006, PhR, 429, 307
Lewis, A., & Bridle, S. 2002, PhRvD, 66, 103511
Mangano, G., Miele, G., Pastor, S., et al. 2005, NucPh B, 729, 221
Mangano, G., & Serpico, P. D. 2011, PhL B, 701, 296
Marulli, F., Carbone, C., Viel, M., Moscardini, L., & Cimatti, A. 2011, MNRAS, 418, 346
Mention, G., Fechner, M., Lasserre, T., et al. 2011, PhRvD, 83, 073006
Moresco, M., Cimatti, A., Jimenez, R., et al. 2012a, JCAP, 08, 006
Moresco, M., Verde, L., Pozzetti, L., Jimenez, R., & Cimatti, A. 2012b, JCAP, 07, 053
Nollett, K. M., & Holder, G. P. 2011, arXiv:1112.2683
Padmanabhan, N., Xu, X., Eisenstein, D. J., et al. 2012, MNRAS, 427, 2132
Parkinson, D., Riemer-Sørensen, S., Blake, C., et al. 2012, PhRvD, 86, 103518
Percival, W. J., & White, M. 2009, MNRAS, 393, 297
Pettini, M., & Cooke, R. 2012, MNRAS, 425, 2477
Riemer-Sørensen, S., Blake, C., Parkinson, D., et al. 2012, PhRvD, 85, 081101
Riess, A. G., Macri, L., Casertano, S., et al. 2011, ApJ, 730, 119
Saito, S., Takada, M., & Taruya, A. 2009, PhRvD, 80, 083528
Schulz, A. E., & White, M. 2006, APh, 25, 172
Simon, J., Verde, L., & Jimenez, R. 2005, PhRvD, 71, 123001
Smith, R. E., Peacock, J. A., Jenkins, A., et al. 2003, MNRAS, 341, 1311
Steigman, G. 2012, arXiv:1208.0032
Stern, D., Jimenez, R., Verde, L., Kamionkowski, M., & Stanford, S. A. 2010, JCAP, 02, 008
Sullivan, M., Guy, J., Conley, A., et al. 2011, ApJ, 737, 102
Taruya, A., Bernardeau, F., Nishimichi, T., & Codis, S. 2012, PhRvD, 86, 103528
Viel, M., Haehnelt, M. G., & Springel, V. 2010, JCAP, 06, 015
Wagner, C., Verde, L., & Jimenez, R. 2012, ApJ, 752, L31
Xia, J.-Q., Granett, B. R., Viel, M., et al. 2012, JCAP, 06, 010